

## A peculiar cyclotron line near 16 keV detected in the 2015 outburst of 4U 0115+63?

Bai-Sheng Liu<sup>1,2,3</sup>, Lian Tao<sup>1,4</sup>, Shuang-Nan Zhang<sup>1,4</sup>, Xiang-Dong Li<sup>2,3</sup>, Ming-Yu Ge<sup>1</sup>, Jin-Lu Qu<sup>1,4</sup>, Li-Ming Song<sup>1,4</sup>, Long Ji<sup>5</sup>, Shu Zhang<sup>1,4</sup>, Andrea Santangelo<sup>5</sup>, Ling-Jun Wang<sup>1</sup>

<sup>1</sup>*Key Laboratory of Particle Astrophysics, Institute of High Energy Physics, Chinese Academy of Sciences, Beijing 100049, China; astrover2012@aliyun.com, taolian@ihep.ac.cn, zhangsn@ihep.ac.cn*

<sup>2</sup>*Department of Astronomy, Nanjing University, Nanjing 210046, China; lixd@nju.edu.cn*

<sup>3</sup>*Key Laboratory of Modern Astronomy and Astrophysics (Nanjing University), Ministry of Education, Nanjing 210046, China*

<sup>4</sup>*University of Chinese Academy of Sciences, Chinese Academy of Sciences, Beijing 100049, China*

<sup>5</sup>*IAAT, University of Tuebingen, Sand 1, Tuebingen D-72076, Germany*

### ABSTRACT

In 2015 October, the Be/X-ray binary 4U 0115+63 underwent a type II outburst, reaching an X-ray luminosity of  $\sim 10^{38}$  erg s<sup>-1</sup>. During the outburst, Nuclear Spectroscopic Telescope Array (*NuSTAR*) performed two Target of Opportunity observations. Using the broad-band spectra from *NuSTAR* (3–79 keV), we have detected multiple cyclotron lines of the source, i.e.,  $\sim 12$ , 16, 22 and 33/35 keV. Obviously, the 16 keV line is not a harmonic component of the 12 keV line. As described by the phase-dependent equivalent widths of these cyclotron lines, the 16 keV and 12 keV lines are two distinct fundamental lines. We propose a model, in which the two line sets are formed in different regions of the same magnetic pole. That is, the former is produced in the outer-region of the column base, and the latter is at a height of  $\sim 1$  km inside the column if the magnetic dipole field is assumed. Thus the magnetic field, deduced from the cyclotron line near 16 keV, is  $\sim 1.4 \times 10^{12}$  G.

*Subject headings:* UAT: Accretion (14); Neutron stars(1108); High mass X-ray binary stars (733); Binary pulsars(153)

## 1. Introduction

In binary systems, by accreting mass from their companion stars, highly magnetized ( $B \gtrsim 10^{12}$  G), rotating neutron stars (NSs) are observed as X-ray pulsars. The interaction between the accretion flow and the magnetic field is one of the key issues in X-ray astronomy. On one hand, the accretion flow tends to be channeled onto the polar cap of the NS along the field lines, and a hotspot or thermal mound is formed, which contributes to a large fraction of X-ray emission (Becker & Wolff 2007). On the other hand, due to the strong field the energies of electrons are quantized according to the Landau level (Mészáros 1992)

$$E_n = n \frac{eB\hbar}{m_e c} \approx 11.6 \text{ keV} \cdot n B_{12}, \quad (1)$$

where  $m_e$  is the mass of an electron,  $n = 1, 2, 3 \dots$  and  $B_{12} = B/10^{12}$  G. The cyclotron resonant scattering feature (CRSF, or commonly referred to as ‘cyclotron line’) of the outgoing photons with these quantized electrons happens in the line-formation region, which naturally explains the absorption features observed in the energy spectra of  $\sim$  forty X-ray pulsars (e.g., Revnivtsev & Mereghetti 2015; Staubert et al. 2019; Truemper et al. 1978; Walter et al. 2015; Wheaton et al. 1979). If the gravitational redshift is considered, the observed energy of the cyclotron line should be  $E_{\text{cyc}} = E_n/(1+z)$ , where  $z$  is the gravitational redshift around the NS. At present, it is the only way to directly measure the magnetic field of NSs. However, the exact location of the line-formation region is still under discussion, and the cyclotron line is occasionally absent in some pulsars. These issues inhibit us from revealing the evolution of the cyclotron line with luminosity (e.g., Doroshenko et al. 2017; Staubert et al. 2017, 2019; Tsygankov et al. 2007).

Furthermore, besides the fundamental line, multiple harmonics were exhibited in the spectra of several X-ray pulsars, e.g., 4U 0115+63 (Santangelo et al. 1999), V 0332+53 (Tsygankov et al. 2006), and GRO J2058+42 (Molkov et al. 2019). From these harmonics, we can infer the fundamental line by calculating the minimal energy gap between them, which is of vital importance to the measurements of the magnetic fields and further studies on X-ray pulsars. In our work, we mainly study the multiple absorption features of 4U 0115+63.

4U 0115+63, locating at  $\sim 7$  kpc (Negueruela & Okazaki 2001), is a Be/X-ray binary (Johns et al. 1978), and its orbital parameters have been measured (orbital period  $P_{\text{orb}} \sim 24.3$  d, eccentricity  $e \sim 0.34$ , Rappaport et al. 1978). It consists of a  $\sim 3.61$  s accreting pulsar (Cominsky et al. 1978) and a Be star. Like other transient Be/X-ray binaries, 4U 0115+63 had undergone several outbursts, during which the fundamental line and several harmonics were detected (e.g., Boldin et al. 2013; Ferrigno et al. 2009; Li et al. 2012; Santangelo et al. 1999; Tsygankov et al. 2007). Especially, for the first time a peculiar cyclotron line near 15 keV was probed simultaneously with those near 11, 20 and 33 keV, and was considered as the other fundamental line (Iyer et al. 2015). If two distinct fundamental lines are detected simultaneously, it is unclear where they are

produced, and from which one the magnetic field can be measured. However, the robustness of the peculiar absorption feature needs further confirmation. On one hand, the signal to noise (S/N) of the observation data, obtained from the joint observations of *Suzaku* and *RXTE*, is somewhat low, since different systematic errors introduce extra uncertainties. On the other hand, the 11 keV line is detected at a low level of significance ( $3.5\sigma$ ), which makes the coexistence of the two line sets doubtful. That is, observations of both line sets with a higher S/N with the same telescope are needed.

In this work, by analyzing two pointing observations of 4U 0115+63 during the 2015 outburst, obtained by the Nuclear Spectroscopic Telescope Array (*NuSTAR*), we try to study the complicated cyclotron lines. *NuSTAR* performs X-ray observations in 3–79 keV, displaying energy resolution of 400 eV (full width at half maximum) at 10 keV and 900 eV at 68 keV. Its inherently low background makes the telescope detect hard X-ray sources with an improvement in sensitivity by 100 times as high as other instruments (Harrison et al. 2013). Its time resolution ( $2 \mu\text{s}$ ) and dead time (2.5 ms) further allow us to obtain observation data with high quality and to analyze pulse phase-resolved energy spectra conveniently. Thus these two *NuSTAR* observations are helpful to confirm the robustness of the peculiar CRSF and reveal its nature. From phase-dependent equivalent widths of the measured CRSFs and the physical model of the accretion column, we can infer the formation processes of these lines. In Section 2, we describe the observation and data reduction. In Section 3, we present details of the spectral fitting, and test the robustness of the peculiar cyclotron line. In Section 4, we try to explain the nature of these confusing absorption lines, and summarize our work.

## 2. Observation and Data Reduction

During the 2015 outburst of 4U 0115+63, *NuSTAR* performed a Target of Opportunity (ToO) observation of 4U 0115+63 on 2015 October 22 and 30 (ObsIDs 90102016002 and 90102016004, hereafter abbreviated as ObsIDs 002 and 004), respectively. The data is obtained with the focal plane module telescopes (FPMA and FPMB). The net exposure times of the two observations are  $\sim 8.6$  and 14.6 ks, respectively. Figure 1 displays the details of these ToO observations during the 2015 outburst (described by *Swift*/BAT), i.e., these *NuSTAR* observations are performed in the peak and decay of the outburst, respectively.

Following the analysis guide of *NuSTAR* data, we first employ the `nupipeline` task (v 0.4.6) of the software `NUSTARDAS` (v 1.8.0, packaged in `HEASOFT` v 6.23) to filter and calibrate the event data, using *NuSTAR* Calibration data base (CALDB; released on Oct. 22 2018)<sup>1</sup>. Secondly, we utilize the `nuproducts` task to extract source (and background) light curves and spectra from the cleaned FPMA and FPMB data, and response files. We obtain the source products using a circular region of 160 arcsec around the source position, and the background products using a circular region of 130 arcsec around a position away from the source region. Thirdly, we group the FPMA and FPMB energy spectra via the `grppha` task with  $\geq 50$  counts per channel bin.

### 3. Spectral Analysis

#### 3.1. Spectral Fitting

To study the cyclotron absorption of the Be/X-ray binary 4U 0115+63 in the giant outburst, we analyze the phase-averaged spectra in 3–79 keV. For ObsID 002 or 004, the FPMA and FPMB energy spectra are fitted together, and the cross normalization factors are adopted, i.e., the factor for FPMA is fixed at 1.0, and that for FPMB is free (with uncertainty of 1–2%, in good agreement with [Madsen et al. 2015](#)). Other parameters for both spectra are tied, respectively.

The broad-band spectra are tentatively fitted with the commonly discussed models. In order to find the interstellar absorption, we adopt the `TBabs` model in `XSPEC` (v 12.10.0) by setting abundances and cross-sections in accordance with those of [Wilms et al. \(2000\)](#) and [Verner & Yakovlev \(1995\)](#), respectively. Since the calibrated spectra below 3 keV are not available here, we fix the absorption column ( $N_{\text{H}}$ ) at  $1.2 \times 10^{22} \text{ cm}^{-2}$  in all fits unless specified ( $\sim (0.5 - 2) \times 10^{22} \text{ cm}^{-2}$ , see [Ferrigno et al. 2009](#); [Iyer et al. 2015](#); [Tsygankov et al. 2016](#)). To fit an absorption feature, we can use a multiplicative gaussian (In `XSPEC` we define a multiplicative model `mgabs` using the function  $1 - \tau \exp[-\frac{(E-E_{\text{cyc}})^2}{2\sigma^2}]$ . See [Mihara et al. 1990](#); [Ferrigno et al. 2009](#); [Doroshenko et al. 2017](#); [Staubert et al. 2019](#)), a fake-Lorentzian (`cyclabs`) or an exponential gaussian model (`gabs`) (e.g., [Nakajima et al. 2010](#); [Müller et al. 2013](#); [Staubert et al. 2019](#)). Here we only adopt model `mgabs` since the other two models may cause some shift in the measured line center or some residuals around the fitted line (see discussions in [Doroshenko et al. 2017](#)).

---

<sup>1</sup>Here we execute the tasks of `nupipeline` and `nuproducts` two times. In the repeated procedure, the keyword `statusexpr` of “STATUS==b0000xxx00xxx000” is considered since in the preliminary processing the incident rate of the light curves with `binsize=1 s` exceeds 100 counts per second (see [https://heasarc.gsfc.nasa.gov/docs/nustar/nustar\\_faq.html](https://heasarc.gsfc.nasa.gov/docs/nustar/nustar_faq.html)).

First, we fit the spectra of ObsID 002 using a `compTT` model. As shown in the left panel ‘a’ of Fig. 2, a significant soft excess is always detected, when different values of  $N_{\text{H}}$  ( $\sim (0.5 - 2) \times 10^{22} \text{ cm}^{-2}$ ) are considered. Adding a low temperature `bb` component significantly improves the spectral fit with  $\Delta\chi^2 \gtrsim 11000$ . An emission line near 6.5 keV, three narrow absorption lines ( $\sim 23, 35$  and 48 keV) and a broad absorption feature ( $\sim 10 - 20$  keV) become apparent in the residuals (see the left panel ‘b’). We then add a `gaussian` and four `mgabs` components to fit these features, which leads to a substantial decrease in  $\chi^2$  (see the left panel ‘c’). Upon closer inspection, we find two small dips in the residuals near 12 keV and 16 keV. The line features are likely related to the poor modelling of the absorption feature in 10 – 20 keV. We suspect that there are two narrow absorption lines rather than a broad one. Therefore, we test the fit by adding another line, and finally obtain a very good fit (see the right panel of Fig. 2) with  $\chi^2/\text{dof} = 1828/1731$  (degree of freedom) and  $\Delta\chi^2 \sim 100$ . In summary, we have detected four harmonics ( $\sim 12, 23, 35$  and 48 keV) and a peculiar one ( $\sim 16$  keV, not a harmonic component of the 12 keV line. See also Roy et al. 2019) in ObsID 002, even when we adopt different values of  $N_{\text{H}}$  ( $\sim (0.5 - 2) \times 10^{22} \text{ cm}^{-2}$ ). If each CRSF is fitted by model `cyclabs` or `gabs`, the absorption feature near 16 keV can still be identified.

Then we repeat the above procedure using some power-law based models (phenomenological ones, see Müller et al. 2013; Staubert et al. 2019), e.g., the simple cutoff power-law (`cutoffpl`), a power-law with a high energy cutoff (`HEcut`), that with a ‘Fermi-Dirac’ cutoff (`FDcut`), or a sum of a negative and positive power-law multiplied by an exponential cutoff (`NPEX`). We still detect the abnormal CRSF near 16 keV in the fit using any of these power-law based models (see Fig. 3), even when model `cyclabs` or `gabs` is applied. If the residual near 16 keV is additionally fitted as a CRSF, the fit is obviously improved as compared to that in Fig. 3, e.g.,  $\chi^2$  of model `cutoffpl`, `NPEX`, `HEcut` and `FDcut` based fittings are reduced by  $\sim 109, 131, 53$  and  $357$ , respectively.

Similarly, in ObsID 004, aside from the harmonic CRSFs ( $\sim 12, 22$  and  $33$  keV), a peculiar one near 16 keV is again detected (see Tbl. 1), when each model used in ObsID 002 is considered.

However, the absorption feature at  $\sim 16$  keV might be related to the so-called “10 keV feature”, described by a wide-`gaussian` profile (e.g., Coburn et al. 2001; Ferrigno et al. 2009; Müller et al. 2013; Staubert et al. 2019). That is, if each of the above fits contains an additive wide-`gaussian` component (see Tbl. 1), the peculiar absorption line at  $\sim 16$  keV would not be detected (see also Fig. 4). Thus, the detected absorption lines are all harmonic, e.g.,  $\sim 12, 23$  and  $33/35$  keV. Even though in the fit including a wide-`gaussian` component the statistical  $\chi^2/\text{dof}$  decreases a little bit accordingly, the wide-`gaussian` profile is associated with unknown physics, besides reflecting the possible distribution of the thermal atoms (e.g., Staubert et al. 2019). Therefore we treat the residual near 16 keV as a CRSF, unless future observations can obtain some astrophysical evidence relating to the wide-`gaussian` model.

### 3.2. Robustness of the 16 keV line

In the above analyses, we have described the details about the detection of multiple cyclotron lines in 4U 0115+63. Especially, we have detected an anomalous CRSF ( $\sim 16$  keV) in both *NuSTAR* observations. Although the similar multiple CRSFs (especially that near 15 keV) in the 2011 outburst have been reported by Iyer et al. (2015), due to higher performance of *NuSTAR*, the CRSFs in our work are measured with a higher S/N. Obviously, the 16 keV line can not be treated as a harmonic component (the fundamental) of the 12 keV (23 keV) line. It seems that the cyclotron line near 16 keV is a distinct fundamental line, unless an absorption line near 5 keV exists, or the 16 keV line is a minor product of the 12 keV line. Therefore, the nature of these two sets of cyclotron lines should be studied, e.g., whether they are formed in the same region or not. Then the cyclotron line near 35 keV (48.5 keV) may also be the first (second) harmonic of the 16 keV line, besides being the second (third) harmonic of the 12 keV line. In Section 4.2, by analyzing the phase-dependent equivalent widths of these cyclotron lines and physical model of the accretion column, we try to answer these questions.

Before modelling the 12 and 16 keV lines, we should check their robustness of detection. By fitting only four (three) CRSFs in ObsID 002 (004), we can roughly estimate the significance from observation data. Our fit tends to fit CRSFs near 12 and 16 keV rather than the harmonics (i.e.,  $\sim 12$  and 23 keV), since the former scheme produces a smaller value of  $\chi^2/\text{dof}$  or a group of satisfactory parameters. For example, using the `compTT` dependent model in ObsID 002, we obtain  $\chi^2/\text{dof}$  of 1851.3/1734 and 1924.78/1734 for the scheme fitting the lines at 11.9, 16.2, 23.2 and 34.8 keV and that fitting the lines at 13.3, 20.8, 35.1 and 47.5 keV, respectively. That is, the absorption features near 12 and 16 keV should not be ignored (see also the right panel of Fig. 2).

In order to further confirm the robustness of the CRSF near 16 keV, we perform the following simulations and fitting-statistics. Briefly, the 16 keV line is not involved to produce the simulated spectra, and due to the statistical fluctuations its possible detection from the simulated spectra is analyzed. The details are described as follows. (i) Basing on the physical model `compTT+gauss+bb` (modified by `TBabs` and four `mgabs` components), we simulate  $10^5$  spectra using script `fakeit` in *XSPEC* package. Besides the response matrix files and auxiliary response files (for FPMA and FPMB) of ObsID 002, the best parameters for the spectrum in Tbl. 1 (except those of the 16 keV line) are applied. Additionally, the exposure durations of ObsID 002 (8.58 and 8.88 ks for FPMA and FPMB, respectively) and statistical (Poisson) noise are considered to produce simulated source and background spectra. (ii) Applying model `compTT+gauss+bb` absorbed by `TBabs` and four `mgabs` components, we fit the simulated spectra and obtain their  $\chi^2$ . By including another `mgabs` component with an initial trial  $E_{\text{cyc}} = 16.20$  keV (varying between 15 and 17 keV) and a fixed line width of 3.17 keV, we again fit the spectra, and calculate  $\Delta\chi^2$  as compared to the former fit. Then the number distribution of these  $\Delta\chi^2$  is shown in panel ‘a’ of Fig.



5. As illustrated in the figure, none of these simulated spectra displays a  $\Delta\chi^2$  close to that of the observation ( $\sim 103.8$ ). That is, if four harmonic lines ( $\sim 12, 23, 35$  and  $48$  keV) are detected in the observed data, the probability of nonexistence of the  $16$  keV line is lower than  $10^{-5}$ .

Then we repeat the above simulation to verify the robustness of the  $12$  keV line, and obtain a similar  $\Delta\chi^2$  distribution in panel ‘b’ of Fig. 5. In the energy band  $11$ – $13$  keV of the simulated spectra, we can not detect an assumed  $12$  keV line with  $\Delta\chi^2$  close to that of the observation ( $\sim 173.0$ ). Therefore, the simultaneous detection probability of the  $12$  keV line with other four cyclotron lines ( $\sim 16, 23, 35$  and  $48$  keV) is greater than  $99.999\%$  in the observed data.

#### 4. Discussion and conclusion

In 4U 0115+63, two cyclotron lines near  $12$  keV and  $20$  keV were first detected by *HEAO* in the 1978 outburst (Wheaton et al. 1979; White et al. 1983) and again in the 1990 outburst (by *GINGA*, Mihara et al. 1998), and a single line around  $17$  keV appeared in the 1991 outburst. In different epochs of the 1999 outburst the second ( $\sim 33$  keV), third ( $\sim 49$  keV) and fourth ( $\sim 57$  keV) harmonics were obtained by *Rossi X-Ray Timing Explorer* (Heindl et al. 1999), *BeppoSAX* (Santangelo et al. 1999) and *BeppoSAX* (Ferrigno et al. 2009), respectively. These absorption lines were further confirmed in more outbursts, observed by other detectors (e.g., Boldin et al. 2013; Li et al. 2012). In the 2011 outburst, among detected CRSFs ( $\sim 11, 15, 20$  and  $33$  keV), the  $15$  keV line is not a harmonic of the  $11$  keV line (Iyer et al. 2015), and the similar situation happened again in the 2015 outburst (see this work and Roy et al. 2019).

In order to reveal the nature of these complicated cyclotron lines observed in the 2015 outburst, we study the pulse phase-resolved spectra. Basing on *NuSTAR* observations, we obtain the phase-resolved spectra in 10 phase bins with equal width, and fit these spectra using the `bb+gauss+compTT` based model. During the fitting, we assume the detections of all CRSFs in each bin by fixing their energies and widths to those of the phase-averaged spectra, respectively, beside fixing  $\sigma_{\text{Fe}}$  accordingly (see Tbl. 1). Then we calculate the phase-dependent equivalent widths (EWs) of the CRSFs (see Fig. 6. Since the line near  $48$  keV is not detected in ObsID 004, we only study other CRSFs) using the following equation (based on model `mgabs`),

$$\text{EW (keV)} = \int_{E_1}^{E_2} \tau \exp\left[-\frac{(E - E_{\text{cyc}})^2}{2\sigma^2}\right] dE, \quad (2)$$

where  $\tau$  and  $\sigma$  are the line depth and width, respectively. For further discussions, we pick up two energy-dependent pulse profiles ( $8$ – $14$  and  $14$ – $19$  keV), each of which is affected by the cyclotron absorption (see the CRSF-corrected and observed profiles in panels ‘N’ and ‘a’ of Fig. 6, respectively).

Obviously, as depicted in Fig. 6, every CRSF is detected at most of the pulse phases. The details about the phase-dependent EWs are summarized as follows.

- 1) The line-formation region of the 12 keV (16 keV) line is primarily observed at  $\phi \sim 0.6–0.9$  (0.2–0.5), at which the pulse profile for the 8–14 keV (14–19 keV) band has a hump, and displays significant cyclotron absorption (see panels ‘N’ and ‘a’ of Fig. 6). At  $\phi \sim 0.9–1.1$  the 16 keV line has another peak EW (e.g., in ObsID 004), where no obvious pulse is detected. Additionally, EW of the 16 keV line is larger than that of the 12 keV line.
- 2) As for the first harmonic of the 12 keV line, the 22 keV line reaches its peak EW at  $\phi \sim 0.2–0.5$  and 0.6–0.9. Especially, at  $\phi \sim 0.2–0.5$  the significant absorption near 22 keV conflicts with the weakness of the 12 keV line, distinct from the situation at  $\phi \sim 0.6–0.9$ .
- 3) As for the second (first) harmonic of the 12 keV (16 keV) line, the absorption line near 33/35 keV becomes very strong at  $\phi \sim 0–0.3$  and 0.6–0.9, but very weak at  $\phi \sim 0.3–0.5$  and 0.9–1.0. Unlike the situation at  $\phi \sim 0.6–0.9$ , at  $\phi \sim 0–0.3$  no component of the 12 keV or 16 keV line set arrives at its peak EW.

Therefore, we believe that two sets of cyclotron lines (fundamental lines of  $\sim 12$  keV and 16 keV, respectively) coexist in the 2015 outburst. First, the formation of the 12 keV and 16 keV lines are not affected by each other. Until now no evidence indicates that an absorption feature near 5 keV is detected (i.e., the two lines are not harmonic), or that the 16 keV line is the by-product of the 12 keV line. Secondly, the 12 keV and 16 keV lines should be formed in distinct regions, since their EWs show different pulse phase dependence, respectively (see Fig. 6). In the following, we further discuss the formation of these distinct line sets using the physical model of the accretion column.

#### 4.1. The physical model of the accretion column

In a X-ray pulsar, most of its X-ray emission comes from the accretion column (Becker & Wolff 2007), and the cyclotron absorption would happen if the continual emission is absorbed by the quantized electrons. Thus the astrophysical processes occurring in the accretion column should be analyzed beforehand.

During a bright outburst (see Eq. (32) in Becker et al. 2012), the fast falling accretion flow is easily braked by the upward radiation from the thermal mound, and an accretion column is gradually formed, inside which the radiation pressure dominates. At the column top, the equilibrium between upward diffusion of radiation and downward advection of the flow is achieved, and upward photons are trapped inside the column. In the column, before reaching the sonic point the



accretion flow freely falls, and encounters the scatter of the upward photons especially in the region below the sonic point (e.g., [Becker & Wolff 2007](#); [Becker et al. 2012](#)). At the bottom of the column, the flow is gathered in the hot mound, where most of radiation is created (i.e., blackbody, cyclotron and bremsstrahlung radiation). Due to being trapped by the advection of the accretion flow and the scatter of the downward hot gas, the radiation tends to escape from the wall of the column (a fan beam). Thus no pencil beam is produced at the top of the column, when the X-ray luminosity is higher than a critical value (see Eq. (32) in [Becker et al. 2012](#)).

It is the scattering cross-section of electrons that affects their interaction with photons and the propagation of photons. In strong magnetic field ( $\gtrsim 10^{12}$  G), the cross-section for low-energy photons ( $E < E_{\text{cyc}}$ ) depends on the field strength, propagation angle with respect to the field and photon energy ([Arons et al. 1987](#); [Becker & Wolff 2007](#); [Becker et al. 2012](#)). The cross-sections parallel ( $\sigma_{\parallel}$ ) and perpendicular ( $\sigma_{\perp}$ ) to the magnetic field can be described, respectively, by (see discussions in [Becker & Wolff 2007](#))

$$\begin{aligned}\sigma_{\parallel} &\approx \left(\frac{E}{E_{\text{cyc}}}\right)^2 \sigma_{\text{T}}, \\ \sigma_{\perp} &\approx \sigma_{\text{T}},\end{aligned}\tag{3}$$

where  $\sigma_{\text{T}}$  is the Thomson cross-section. Thus low-energy photons ( $E < E_{\text{cyc}}$ ) tend to escape from the wall in a direction close to the field line due to  $\sigma_{\parallel} < \sigma_{\perp}$ . That is, along the magnetic field line more low-energy photons are observed (a ‘‘pencil-like’’ beam), which corresponds to the main peak in the pulse profile for the low-energy band (e.g., 8–14 keV, see panel ‘a’ of Fig. 6). If the ratio of photons undergoing cyclotron absorption is very low, the pulse profile (especially its hump) is hardly affected by the cyclotron absorption.

In addition, some photons from the fan beam are scattered by the NS surface (heating the NS), and some other photons irradiate the upper accretion flow (close to the column axis). Affected by the advection of the accretion flow and the light deflection, the irradiation is reprocessed in the accretion flow, and possibly causes the formation of a narrow ‘‘anti-pencil’’ beam ([Sasaki et al. 2012](#)). The narrow pencil beam appears in a direction of  $\sim 0.5$  pulse phase away from that of the accretion column (see also [Sasaki et al. 2010](#)).

## 4.2. About the absorption feature near 16 keV

### 4.2.1. Test the previous models

Before proposing a new model for the formation of the peculiar cyclotron line near 16 keV, we introduce the previous models in [Iyer et al. \(2015\)](#), and evaluate their viabilities.

In the previous work analyzing the 2011 outburst (Iyer et al. 2015), the complicated cyclotron lines, classified into two distinct line sets, are believed to be formed in different regions, which is in consistence with our analysis. They proposed two possibilities to explain the detected lines.

The first case depends on the dipolar structure of the NS magnetic field, where the 11 and 15 keV line sets are formed in the pencil beam (the top of the shock) and fan beam (the base of the hot mound), respectively. The model can describe the formation of the two possible sets of cyclotron lines in GX 301–2 (Fürst et al. 2018). However, the model is in disagreement with the bright outburst (see Eq. (32) in Becker et al. 2012)<sup>2</sup>. First, the pencil beam can not be formed at the top of the accretion column where upward photons are trapped by the advection of the accretion flow. Moreover, the column top ( $\sim 10$  km, see Eq. (16) in Becker et al. 2012) is higher than the location ( $\sim 1.0$  km, assuming  $B \propto R^{-3}$  and on NS surface  $E_{\text{cyc}} \simeq 16$  keV, where  $R$  is the distance to the NS center) at which the 12 keV line set is formed.

In the second case, Iyer et al. (2015) supposed that the two sets of CRSFs are formed on two poles of the NS with nondipolar magnetic fields, respectively, supported by the following studies. (a) By decomposing the energy-dependent pulse profiles of 4U 0115+63 at different levels of luminosities, Sasaki et al. (2012) derived that the magnetic axes of the two poles are misaligned (offset by  $\sim 60^\circ$ ). In the distorted configuration, the local magnetic fields of the two poles might be distinct. (b) Given that each energy-dependent pulse profile ( $\lesssim 50$  keV) has double peaks (a main and minor one), Iyer et al. (2015) analyzed the energy-dependent phase lags of each peak by defining a reference pulse profile (see also Ferrigno et al. 2011). The significant negative phase-shifts of the main (minor) peak were detected at energies of  $\sim 11, 23$  and  $39$  keV ( $16$  and  $30$  keV), respectively, which indicate the related CRSFs. Provided that each peak in the pulse profile of 4U 0115+63 stands for the emission from one pole, they concluded that the two sets of CRSFs are formed in the two poles, respectively. However, some assumptions in their analysis are inconsistent with the observation in the 2015 outburst, e.g., some energy-dependent pulse profile displays more than two peaks (see panel ‘002-a’ of Fig. 6). In addition, the two line sets might be produced in the fan and pencil beams, respectively, if these radiation regions contribute to different humps in the pulse profile accordingly (e.g., Sasaki et al. 2012; Iwakiri et al. 2019, and in our model a ‘pencil-like’ and fan beams). We thus consider that the two-poles model does not provide a unique explanation to the detected cyclotron lines in 4U 0115+63, and in the following we propose an alternative model for the formation of the two line sets from two radiation-regions in the same pole.

---

<sup>2</sup>For ObsIDs 002 and 004, the 0.1–100 keV luminosities are, respectively,  $1.08 \times 10^{38} \text{ erg s}^{-1} (d/7 \text{ kpc})^2$  and  $7.28 \times 10^{37} \text{ erg s}^{-1} (d/7 \text{ kpc})^2$ . In the 2011 outburst, the 3–50 keV luminosities  $\gtrsim 2 \times 10^{37} \text{ erg s}^{-1}$ .

#### 4.2.2. Our model

In our model, the two line sets are formed in different regions of the same magnetic pole, respectively (see the right panel of Fig. 7). The 16 keV line set is formed in the outer-region of the column base (close to the NS surface), and the 12 keV line set is at a higher location inside the column. Therefore basing on  $E_{\text{cyc}} \simeq 16$  keV we obtain the magnetic field of the NS surface ( $\sim 1.4 \times 10^{12}$  G). If a dipolar magnetic field (i.e.,  $B \propto R^{-3}$ ) is satisfied in 4U 0115+63, the 12 keV line set should be formed at a height of  $z \simeq 1$  km in the column<sup>3</sup> since on the NS surface  $E_{\text{cyc}} \simeq 16$  keV. Especially, the 16 keV line set is created in the outer-region of the column base rather than its inner-region, when the continuum radiation around 14–19 keV from the thermal mound passes through the region. Otherwise EW of the 16 keV line would follow a similar phase-dependence to that of the 12 keV line, inconsistent with Fig. 6. Moreover, the continuum radiation in 14–19 keV is easily suppressed by the dense flow in the inner-region of the column base. Here we also assume that the radiation from the other pole is not important.

In order to test our model using the observation in Fig. 6, we further assume that at  $\phi \sim 0.4$  the line of sight is close to the magnetic field line, where we observe a main peak in the pulse profile for the low-energy band (e.g., 8–14 keV, see panels ‘N’ and ‘a’ of Fig. 6). It accords with our prediction that low energy photons ( $E < E_{\text{cyc}}$ , scattered inside the column) tend to diffuse along the field line due to  $\sigma_{\parallel} < \sigma_{\perp}$  (see Eq. (3)), i.e., forming a “pencil-like” beam. As discussed in the previous studies (Sasaki et al. 2010, 2012), in the direction of the column axis a portion of the pencil-like beam is easily reprocessed by the accretion flow (see the pencil-like beam ‘B’ in the left panel of Fig. 7), and hence the observed radiation is a hollow pencil-like beam (see the pencil-like beam ‘A’). Near phase  $\phi \sim 0.4$  ( $\sim 0.2$ – $0.5$ ), in the pencil-like beam we detect the 16 keV line (see panel ‘b’ of Fig. 6). The line is produced when the continuum radiation of 14–19 keV from the thermal mound passes through the outer-region of the column base. At about 0.25 phase away from the accretion column ( $\phi \sim 0.6$ – $0.9$ ), in the fan beam we detect the 12 keV line set, which is produced when the continuum radiation of 8–14 keV from the thermal mound passes through the region at  $z \sim 1$  km in the column (lower than the sonic point,  $z \sim 1.6$  km, see Eqs. (23), (31), (A14) & (A17) in Becker et al. 2012). Furthermore, due to the advection of the accretion flow and gravitational light deflection, the reprocessed pencil-like beam in the accretion flow (see the pencil-like beam ‘B’ in the left panel of Fig. 7) produces a narrow anti-pencil beam, which preserves the absorption feature near 16 keV from the pencil-like beam. Therefore, on the back side of the accretion column ( $\phi \sim 0.9$ – $1.1$ ), in the anti-pencil beam we detect the 16 keV line

---

<sup>3</sup>The location is higher than the emission region at which most photons are scattered by hot electrons and escape from the column wall ( $z \simeq 0.23$  km, see Eq. (40) and discussions in Becker et al. 2012). That is, it is much easier for the quantized electrons at  $z \simeq 1$  km (not  $z \simeq 0.23$  km) to undergo the cyclotron absorption, as compared to those in other regions.

again (especially, see panel ‘004-b’ of Fig. 6). Additionally, due to a higher density of quantized electrons in the line-formation region, the absorption feature near 16 keV (at  $\phi \sim 0.2–0.5$ ) is deeper than that near 12 keV ( $\phi \sim 0.6–0.9$ ).

Then we apply our model to explain the observations of the other harmonic components as follows.

- 1) At  $\phi \sim 0.6–0.9$ , EWs of the 12 keV line and its first harmonic ( $\sim 22$  keV) both arrive at their peaks (see panels ‘b’ and ‘c’ in Fig. 6). However, at  $\phi \sim 0.2–0.5$  the weakness of the 12 keV line is in conflict with the significant absorption near 22 keV, which is observed in the pencil-like beam. The discrepancy is consistent with the previous studies (Araya-Góchez & Harding 2000; Schönherr et al. 2007), i.e., it is the de-excitation of the thermal electrons and photon filling near the energy of the fundamental line that weaken the strength of the fundamental line. At  $\phi \sim 0.2–0.5$  the count rate in the 8–14 keV band is  $\sim 15$  times of that in the 19–27 keV band, in accordance with the property of the pencil-like beam (see Sec. 4.1). Thus among photons in 8–14 keV, the ratio of those being absorbed is very small, as compared to the situation of photons in 19–27 keV, which causes a shallower absorption feature near 12 keV.
- 2) The phase-dependent EW of the 33/35 keV line becomes complicated, in that the line is either the first harmonic of the 16 keV line, or the second harmonic of the 12 keV line. At  $\phi \sim 0.6–0.9$ , the phase-dependent EW of the 33/35 keV line is similar to those of the 12 keV and 22 keV lines, i.e., the 12 keV line set is the main contribution to the detection of the 33/35 keV line. At  $\phi \sim 0–0.3$ , the situation indicates that the 16 keV and 12 keV line sets both contribute to the formation of the 33/35 keV line, and due to a higher ratio of photons being absorbed in 30–40 keV EW of the 33/35 keV line is larger than that of the 12 keV or 16 keV line. Additionally, at  $\phi \sim 0.3–0.5$  (0.9–1.0), due to lack of high-energy photons (and/or high-energy electrons) in the direction undergoing the cyclotron absorption, the absorption line near 33/35 keV is very weak.

More observations are also consistent with our model, e.g., (i) each cyclotron line is created in a region close to the continual radiation region (see the right panel of Fig. 7), in that the cyclotron line can be detected in most pulse phases (Fig. 6). (ii)  $\frac{\Delta B}{\Delta z}$  in each line-formation region should be small (see the right panel of Fig. 7), otherwise the cyclotron line would be much wider than the observed, or even hardly be observed.

Even though centroid energies of these two fundamental lines both decrease with the decaying outburst in our work (see Tbl. 1), no final conclusion can be drawn. From our model, we infer that the centroid energy of the 16 keV line should not vary with luminosity, and it is unclear whether the cyclotron absorption can happen in the subcritical state (see Eq. (32) in Becker et al. 2012). However, the correlation of the luminosity with the centroid energy of the 12 keV line is complex.

As summarized by previous studies (e.g., [Becker et al. 2012](#); [Doroshenko et al. 2017](#)), two types of correlations between the luminosity and CRSF energy are observed. That is, in the subcritical state a positive correlation is detected, and in the supercritical state an anti-correlation is. We suppose that at different levels of luminosities the luminosity-dependent centroid energy of the 12 keV line should also follow these correlations, respectively.

Future studies are expected to be performed as follows. (1) If the physical nature of the “10 keV feature”, described by a wide-gaussian profile, is confirmed, some methods should be developed to distinguish the “10 keV feature” from the cyclotron line in the energy spectrum. (2) Theoretical calculations should be followed to understand some issues, e.g., the physical properties of these distinct line-formation regions, the effect of the radiation from the other magnetic pole, and the effect of nondipolar magnetic fields. Then we might understand why two line-formation regions appear in 4U 0115+63, and predict the same situation in other accreting pulsars. Our work is helpful to understand more issues of the cyclotron line and the distribution of the magnetic field, e.g., the luminosity-dependence of the cyclotron line energy at different levels of luminosities (e.g., [Doroshenko et al. 2017](#); [Staubert et al. 2017, 2019](#); [Tsygankov et al. 2007](#)). Especially, for different line sets, the luminosity-dependent line energy should satisfy distinct functions, respectively (e.g., [Tsygankov et al. 2007](#); [Boldin et al. 2013](#)).

### 4.3. Conclusion

In our work, we have studied two pointing observations of 4U 0115+63 in the 2015 outburst, obtained by *NuSTAR*. In both observations, we have detected several harmonic CRSFs ( $\sim 12$ , 23 and 33/35 keV) and a peculiar one ( $\sim 16$  keV), similar to those jointly observed in the 2011 outburst by several X-ray detectors ( $\sim 15$  keV, [Iyer et al. 2015](#)). It is clear that the 16 keV line is not a harmonic component of the 12 keV line. We suppose that the fitting residual around 16 keV is not a so-called “10 keV feature”, of which the physical nature is still an open issue (e.g., [Staubert et al. 2019](#)). Then the robustness of the 16 keV line is confirmed. First, because of the high performance of *NuSTAR* the complicated cyclotron lines are detected with a higher S/N and less uncertainty, as compared to the previous observation in [Iyer et al. \(2015\)](#). Secondly, in the fits using physical or phenomenological models, the absorption features near 12 keV and 16 keV are very significant and should be fitted preferentially. Thirdly, our simulations indicate that no simultaneous-detection probability of the 12/16 keV line with other lines is lower than  $10^{-5}$ .

From the pulse phase-dependent equivalent widths of these cyclotron lines (see Fig. 6), we infer that the 12 keV and 16 keV lines are two distinct fundamental lines. In our model, the two line sets are produced in different regions of the same magnetic pole (see Fig. 7). The 16 keV line set is generated in the outer-region of the column base, and its fundamental can be detected in a

direction close to the column axis (the pencil-like beam,  $\phi \sim 0.2–0.5$ ) and on the back-side of the column (the anti-pencil beam,  $\phi \sim 0.9–1.1$ ). Thus the 12 keV line set is produced at an altitude of  $\sim 1$  km inside the column providing that the magnetic field in 4U 0115+63 is dipolar, and its fundamental can be observed in the fan ( $\phi \sim 0.6–0.9$ ) and pencil-like beams ( $\phi \sim 0.2–0.5$ ). Thus the NS magnetic field in 4U 0115+63 should be measured from the line energy  $E_{\text{cyc}} \simeq 16$  keV, i.e.,  $\sim 1.4 \times 10^{12}$  G. Additionally, our model predicts the luminosity-dependent centroid energy of the two fundamental lines as follows. The centroid energy of the 16 keV line is independent of the luminosity, and that of the 12 keV line might follow the positive and negative correlations with the luminosity at different levels of luminosities, respectively.

We are grateful to Prof. Fang-Jun Lu, P. A. Becker, G. K. Jaisawal and M. Yukita for clarifying and helpful comments. This work is supported by Project U1838201, National Key Research and Development Program of China (2016YFA0400803), the Natural Science Foundation of China under grant Nos. 11733009, Y71131005C, 11673023, 11333004 and 11773015 supported by NSFC and CAS. This research has made use of the *NuSTAR* Data Analysis Software (NuSTARDAS) jointly developed by the ASI Science Data Center (ASDC, Italy) and the California Institute of Technology (Caltech, USA), and the software provided by the High Energy Astrophysics Science Archive Research Center (HEASARC).

## REFERENCES

- Araya-Góchez, R. A., & Harding, A. K. 2000, *ApJ*, 544, 1067
- Arons, J., Klein, R. I., & Lea, S. M. 1987, *ApJ*, 312, 666
- Becker, P. A., Klochkov, D., Schönherr, G., Nishimur, O., et al. 2012, *AA*, 544, A123
- Becker, P. A., Wolff, M. T. 2007, *ApJ*, 654, 435
- Boldin, P. A., Tsygankov, S. S., & Lutovinov, A. A. 2013, *Astro. Letters*, 39, 375
- Coburn, W. 2001, Ph.D. Thesis, University of California, San Diego
- Cominsky, L., Clark, G. W., Li, F., Mayer, W., Rappaport, S. 1978, *Nature*, 273, 367
- Doroshenko, V., Tsygankov, S. S., Mushtukov, A. A., et al. 2017, *MNRAS*, 466, 2143
- Ferrigno, C., Becker, P. A., Segreto, A., Mineo, T., & Santangelo, A. 2009, *AA*, 498, 825
- Ferrigno, C., Falanga, M., Bozzo, E., Becker, P. A., et al. 2011, *AA*, 532, A76



- Fürst, F., Falkner, S., Marcu-Cheatham, D., Grefenstette, B., et al. 2018, *AA*, 620, A153
- Harrison, F. A., Craig, W. W., et al. 2013, *ApJ*, 770, 103
- Heindl, W. A., Coburn, W., Gruber, D. E., et al. 1999, *ApJ*, 521, L49
- Iwakiri, W. B., Pottschmidt, K., et al. 2019, *ApJ*, 878, 121
- Iyer, N., Mukherjee, D., Dewangan, G. C., et al. 2015, *MNRAS*, 454, 741
- Johns, M., Koski, A., Canizares, C., et al. 1978, *IAU Circ.*, 3171, 1
- Li, J., Wang, W., & Zhao, Y.-H. 2012, *MNRAS*, 423, 2854
- Madsen, K. K., Harrison, F. A., Markwardt, C. B., et al. 2015, *ApJS*, 220, 8
- Mészáros, P. 1992, *High-Energy Radiation from Magnetized Neutron Stars* (Chicago: Univ. Chicago Press)
- Mihara, T., Makishima, K., & Nagase, F. 1998, *Adv. Space Res.*, 22, 987
- Mihara, T., Makishima, K., Ohashi, T., Sakao, T., & Tashiro, M. 1990, *Nature*, 346, 250
- Molkov, S., Lutovinov, A., Tsygankov, S., Mereminskiy, I., & Mushtukov, A. 2019, *ApJL*, 883, L11
- Müller, S., Ferrigno, C., Kühnel, M., et al. 2013, *AA*, 551, A6
- Nakajima, M., Mihara, T., & Makishima, K. 2010, *ApJ*, 710, 1755
- Negueruela, I., Okazaki, A. T. 2001, *AA*, 369, 108
- Rappaport, S., Clark, G. W., Cominsky, L., Li F., Joss, P. C. 1978, *ApJ*, 224, L1
- Revnivtsev, M., Mereghetti, S. 2015, *Space Sci. Rev.*, 191, 293
- Roy, J., Agrawal, P. C., Iyer, N. K., Bhattacharya, D., et al. 2019, *ApJ*, 872, 33
- Santangelo, A., Segreto, A., Giarrusso, S., et al. 1999, *ApJL*, 523, L85
- Sasaki, M., Klochkov, D., Kraus, U., Caballero, I., Santangelo, A. 2010, *AA*, 517, A8
- Sasaki, M., Müller, D., Kraus, U., Ferrigno, C., Santangelo, A. 2012, *AA*, 540, A35
- Schönherr, G., Wilms, J., Kretschmar, P., et al. 2007, *AA*, 472, 353
- Staubert, R., Klochkov, D., et al. 2017, *AA*, 606, L13

- Staubert, R., Trümper, J., Kendziorra, E., et al. 2019, AA, 622, A61
- Truemper, J., Pietsch, W., Reppin, C., et al. 1978, ApJL, 219, L105
- Tsygankov, S. S., Lutovinov, A. A., Churazov, E. M., Sunyaev, R. A. 2006, MNRAS, 371, 19
- Tsygankov, S. S., Lutovinov, A. A., et al. 2007, Astron. Lett., 33, 368
- Tsygankov, S. S., Lutovinov, A. A., Doroshenko V., Mushtukov A. A., et al. 2016, AA, 593, A16
- Walter, R., Lutovinov, A. A., Bozzo, E., Tsygankov, S. S. 2015, Astron. Astrophys. Rev., 23, 2
- Wheaton, W. A., Doty, J. P., Primini, F. A., et al. 1979, Nature, 282, 240
- White, N., Swank, J., & Holt, S. 1983, ApJ, 270, 711
- Wilms, J., Allen, A., McCray, R. 2000, ApJ, 542, 914
- Verner, D. A., Yakovlev, D. G. 1995, AAS, 109, 125

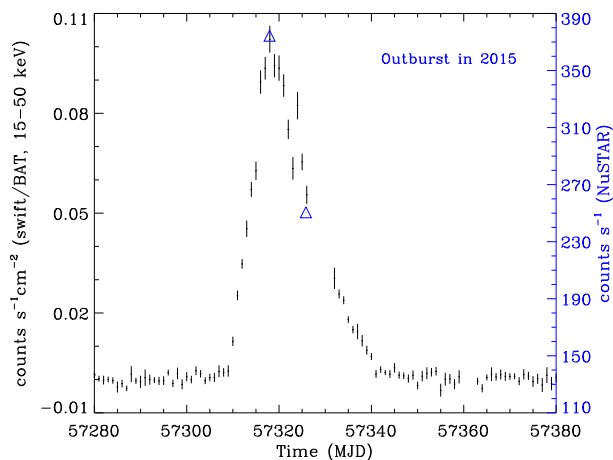


Fig. 1.— The 2015 outburst of 4U 0115+63 monitored by *Swift*/BAT (black points). Two *NuSTAR* observations used in this paper are marked in blue triangles.

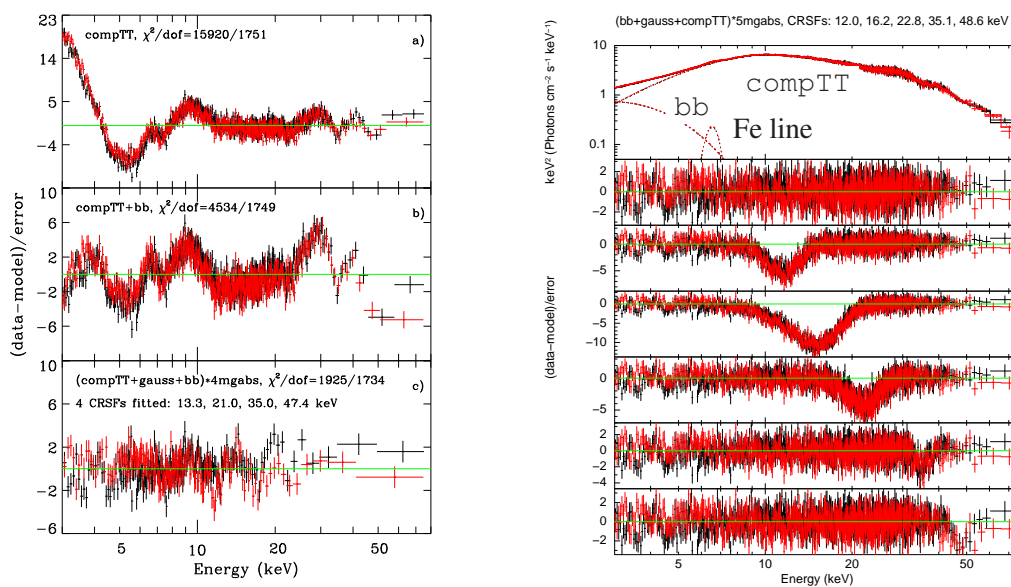


Fig. 2.— Left panels: spectral residuals with respect to different models for ObsID 90102016002. A `compTT` model is used to fit the continuum. Right panels (from top to bottom): energy spectra and model components; spectral residuals for the best-fitting model (`compTT` + `bb` + Gaussian + 5 CRSFs); spectral residuals with one line from the 5 CRSFs (12.0, 16.2, 22.8, 35.1 and 48.6 keV) removed, respectively. Except as specifically described, the following figures show the results from ObsID 90102016002.

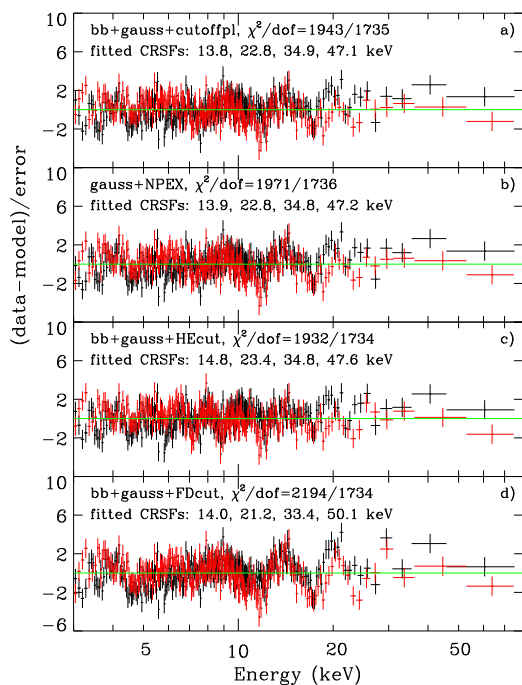


Fig. 3.— Spectral residuals of different continuum models (*cutoffpl*, *NPEX*, *HEcut* or *FDcut*). In order to confirm the presence of the residual near 16 keV, we test different continuum models. In all cases, the line feature around 16 keV is always apparent.

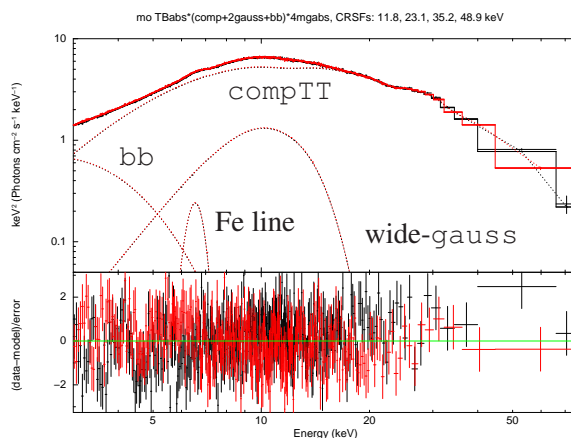


Fig. 4.— Energy spectra and spectral residuals if adding a wide Gaussian around 10 keV in the fitting model.

Table 1. Spectral parameters of the best-fitting models.

Parameters-A <sup>a</sup>	ObsID-002 <sup>b</sup>	ObsID-004	Parameters-B	ObsID-002	ObsID-004
$kT_0$ (keV)	$2.43^{+0.05}_{-0.03}$	$2.66^{+0.05}_{-0.04}$	$kT_0$ (keV)	$1.97^{+0.03}_{-0.04}$	$2.39^{+0.04}_{-0.03}$
$kT_e$ (keV)	$9.34^{+0.28}_{-0.30}$	$11.75^{+0.40}_{-0.38}$	$kT_e$ (keV)	$8.21^{+0.28}_{-0.21}$	$10.53^{+0.40}_{-0.47}$
$\tau_{\text{comp}}$	$1.69^{+0.09}_{-0.09}$	$0.97^{+0.07}_{-0.07}$	$\tau_{\text{comp}}$	$2.54^{+0.12}_{-0.11}$	$1.25^{+0.12}_{-0.11}$
$N_{\text{comp}}$	$0.17^{+0.01}_{-0.01}$	$0.09^{+0.00}_{-0.00}$	$N_{\text{comp}}$	$0.17^{+0.00}_{-0.01}$	$0.12^{+0.01}_{-0.00}$
$E_{\text{Fe}}$ (keV)	$6.51^{+0.04}_{-0.04}$	$6.52^{+0.03}_{-0.03}$	$E_{\text{Fe}}$ (keV)	$6.52^{+0.04}_{-0.03}$	$6.53^{+0.03}_{-0.03}$
$\sigma_{\text{Fe}}$ (keV)	$0.32^{+0.05}_{-0.04}$	$0.26^{+0.04}_{-0.04}$	$\sigma_{\text{Fe}}$ (keV)	$0.34^{+0.05}_{-0.04}$	$0.29^{+0.04}_{-0.04}$
$kT_{\text{bb}}$ (keV)	$0.67^{+0.02}_{-0.02}$	$0.69^{+0.02}_{-0.02}$	$kT_{\text{bb}}$ (keV)	$0.61^{+0.02}_{-0.02}$	$0.62^{+0.02}_{-0.02}$
$R_{\text{bb}}$ (km) <sup>c</sup>	$20.63^{+1.14}_{-1.00}$	$15.93^{+0.86}_{-0.72}$	$R_{\text{bb}}$ (km)	$23.62^{+1.89}_{-1.46}$	$19.82^{+1.41}_{-1.23}$
$E_1$ (keV)	$12.01^{+0.17}_{-0.13}$	$11.85^{+0.20}_{-0.15}$	$E_1$ (keV)	$11.79^{+0.17}_{-0.13}$	$11.73^{+0.16}_{-0.14}$
$\sigma_1$ (keV)	$1.48^{+0.18}_{-0.16}$	$1.62^{+0.18}_{-0.17}$	$\sigma_1$ (keV)	$1.50^{+0.21}_{-0.17}$	$4.53^{+0.22}_{-0.17}$
$\tau_1$	$0.08^{+0.02}_{-0.01}$	$0.10^{+0.03}_{-0.02}$	$\tau_1$	$0.07^{+0.02}_{-0.02}$	$0.67^{+0.01}_{-0.02}$
$E_2$ (keV)	$16.20^{+0.40}_{-0.33}$	$15.67^{+0.28}_{-0.21}$	$E_G$ (keV)	$8.71^{+0.34}_{-0.37}$	$10.06^{+0.09}_{-0.11}$
$\sigma_2$ (keV)	$3.17^{+0.43}_{-0.30}$	$2.89^{+0.27}_{-0.23}$	$\sigma_G$ (keV)	$2.95^{+0.19}_{-0.16}$	$2.54^{+0.10}_{-0.08}$
$\tau_2$	$0.22^{+0.02}_{-0.01}$	$0.30^{+0.02}_{-0.02}$	$N_G$	$0.11^{+0.02}_{-0.01}$	$0.43^{+0.02}_{-0.02}$
$E_3$ (keV)	$22.81^{+0.40}_{-0.33}$	$22.31^{+0.32}_{-0.30}$	$E_2$ (keV)	$23.10^{+0.38}_{-0.24}$	$22.58^{+0.23}_{-0.22}$
$\sigma_3$ (keV)	$2.80^{+0.42}_{-0.38}$	$3.31^{+0.28}_{-0.33}$	$\sigma_2$ (keV)	$1.78^{+0.50}_{-0.29}$	$2.56^{+0.40}_{-0.30}$
$\tau_3$	$0.19^{+0.02}_{-0.02}$	$0.25^{+0.02}_{-0.02}$	$\tau_2$	$0.09^{+0.01}_{-0.01}$	$0.18^{+0.02}_{-0.02}$
$E_4$ (keV)	$35.08^{+0.30}_{-0.40}$	$33.14^{+0.77}_{-0.91}$	$E_3$ (keV)	$35.16^{+0.40}_{-0.42}$	$33.59^{+0.90}_{-0.96}$
$\sigma_4$ (keV)	$1.87^{+0.63}_{-0.55}$	$2.36^{+1.20}_{-0.75}$	$\sigma_3$ (keV)	$2.05^{+0.45}_{-0.44}$	$1.67^{+1.35}_{-0.81}$
$\tau_4$	$0.16^{+0.03}_{-0.03}$	$0.08^{+0.02}_{-0.03}$	$\tau_3$	$0.19^{+0.02}_{-0.04}$	$0.06^{+0.03}_{-0.03}$
$E_5$ (keV)	$48.58^{+2.30}_{-1.44}$	–	$E_4$ (keV)	$48.90^{+1.98}_{-1.20}$	–
$\sigma_5$ (keV)	$4.06^{+2.76}_{-1.68}$	–	$\sigma_4$ (keV)	$6.18^{+3.22}_{-1.13}$	–
$\tau_5$	$0.18^{+0.06}_{-0.06}$	–	$\tau_4$	$0.25^{+0.06}_{-0.04}$	–
$\chi^2/\text{dof}$	1828.0/1731	1955.9/1751	$\chi^2/\text{dof}$	1824.9/1731	1952.2/1751
Null hyp. prob.	$5.2 \times 10^{-2}$	$4.1 \times 10^{-4}$	Null hyp. prob.	$5.7 \times 10^{-2}$	$5.0 \times 10^{-4}$

Note. — The `compTT` model is used to fit the continuum. The table contains four key parameters of model `compTT` (the temperature of input photons  $kT_0$  and thermal electrons  $kT_e$ , photon depth  $\tau_{\text{comp}}$  and normalization  $N_{\text{comp}}$ ), two of `bb` (the blackbody temperature  $kT_{\text{bb}}$  and emission radius  $R_{\text{bb}}$ , assuming a source distance of 7 kpc), two of Fe line (the energy  $E_{\text{Fe}}$  and width  $\sigma_{\text{Fe}}$ ), three of `wide-gaussian` (the energy  $E_G$ , width  $\sigma_G$  and normalization  $N_G$ ), and three of each `CRSF` (the line energy  $E_i$ , width  $\sigma_i$  and depth  $\tau_i$  of the  $i$ -th cyclotron line, where  $i=1, 2, 3, 4, 5$ ). Here errors are calculated at a level of 90% confidence in all cases.

<sup>a</sup>Parameters-A (-B) indicates the results without (with) a `wide-gauss` model.

<sup>b</sup>ObsID-002 (-004) stands for ObsID 90102016002 (90102016004).

<sup>c</sup> $R_{\text{bb}}$  is overestimated, and should be corrected using Compton scattering of the blackbody radiation ( $\sim 7$  km, see discussions in Iyer et al. 2015).

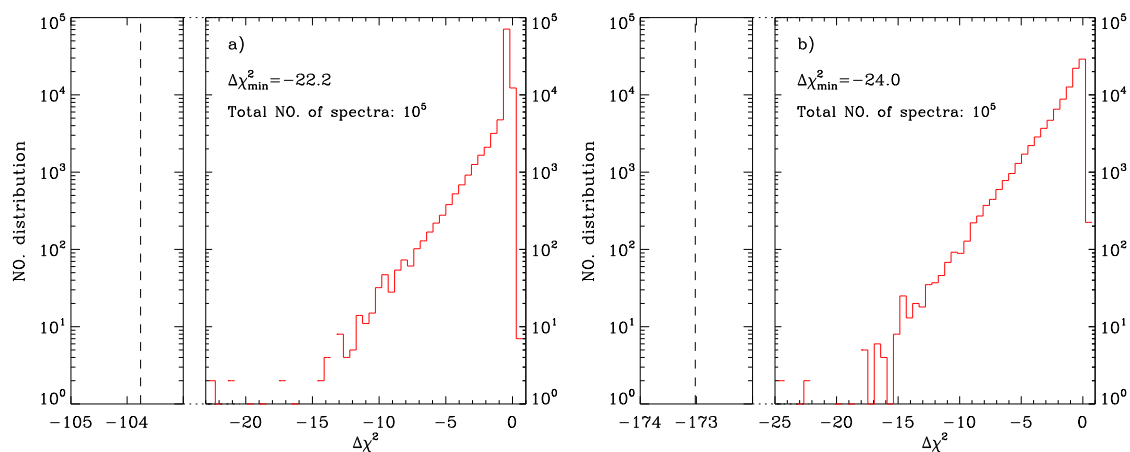


Fig. 5.— Results from the significance simulations. The histograms show  $\Delta\chi^2$  by adding a 16 keV (left panel) or 12 keV (right panel) line to  $10^5$  simulated spectra. The observed  $\Delta\chi^2$  are marked by the dashed lines. A model consisting of `compTT+gauss+bb` and `4 mgabs` components is used to simulate the spectra (see Sec. 3.2 for more details).



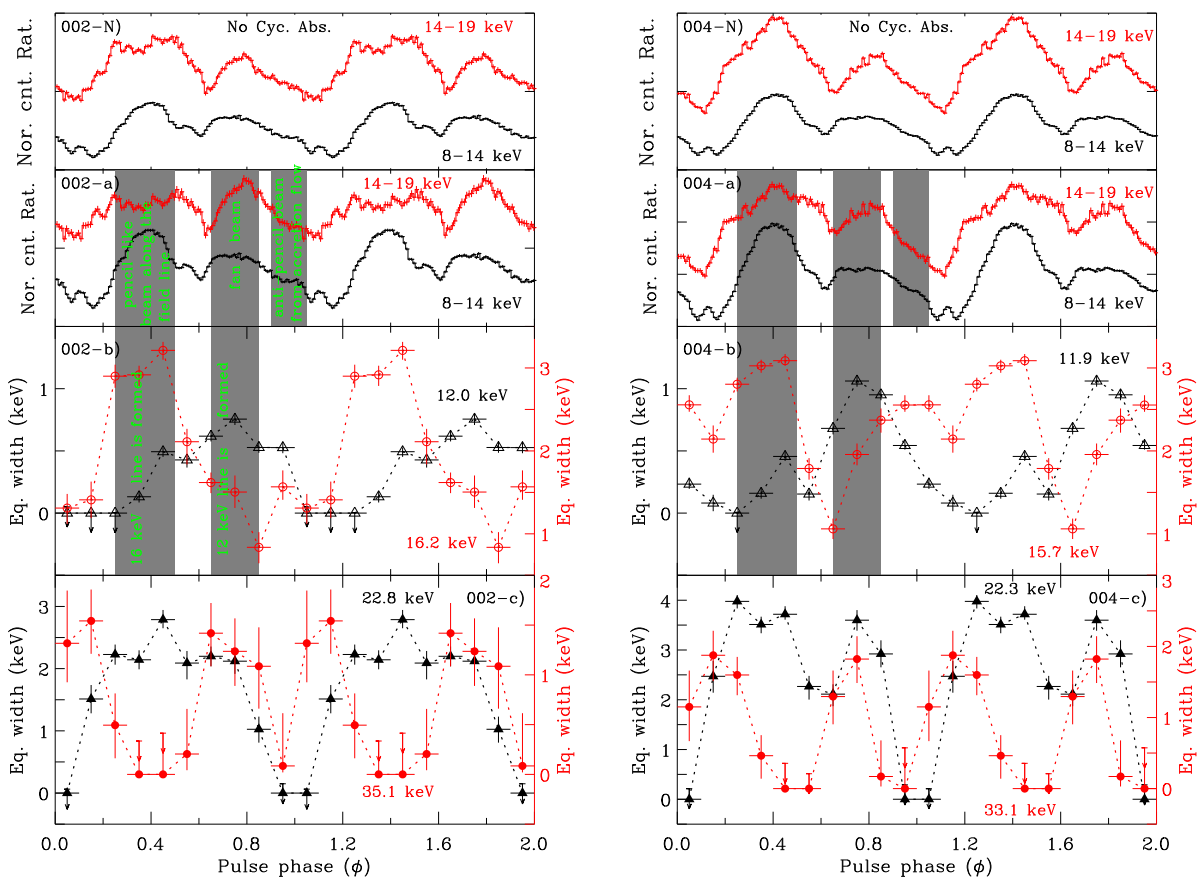


Fig. 6.— Pulse profiles and equivalent widths of the CRSFs for ObsIDs 90102016002 (left panels) and 90102016004 (right panels). The black open triangles, red open circles, black filled triangles and red filled circles indicate the lines of 12, 16, 22 and 33/35 keV, respectively. Different radiation modes (i.e., the pencil-like beam, fan beam and anti-pencil beam) are marked in the observed pulse profiles. For comparison, we also calculate the cyclotron-absorption-corrected pulse profiles in the top panels (panel ‘N’).

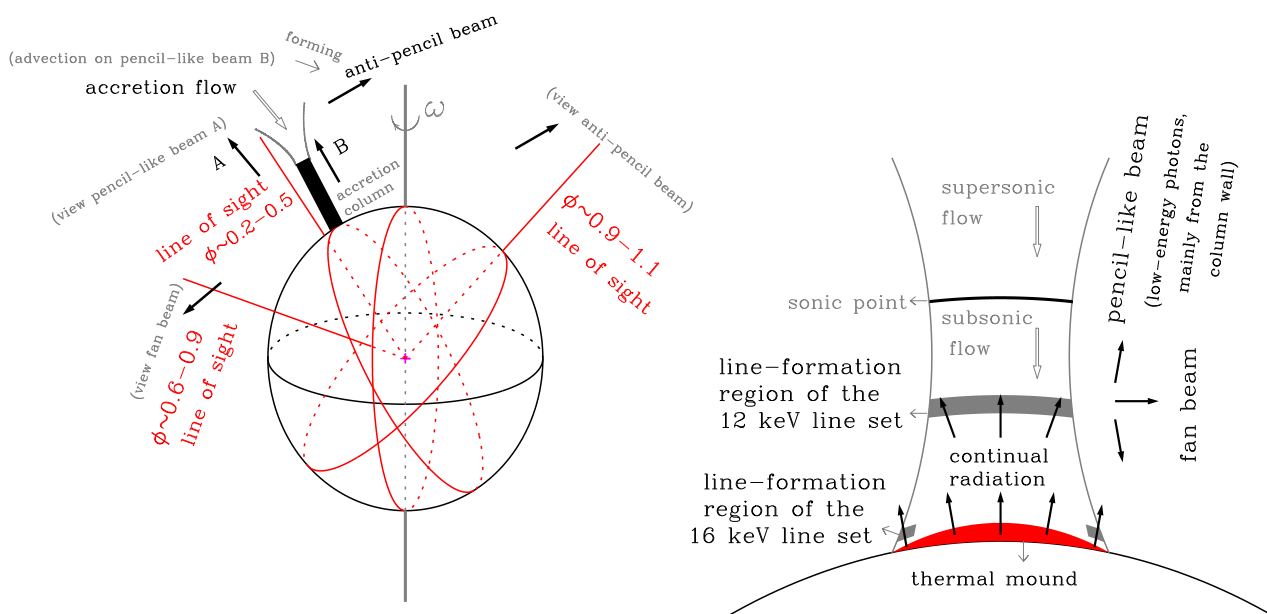


Fig. 7.— Left: schematic of the radiation region.  $\phi \sim 0.2-0.5$ ,  $0.6-0.9$  and  $0.9-1.1$  are three key pulse phases, at which we detect two different sets of cyclotron lines, as shown in Fig. 6. That is, the 16 keV line detected at  $\phi \sim 0.2-0.5$  may be in the pencil-like beam; the 12 keV line at  $\phi \sim 0.6-0.9$  may be in the fan beam; a portion of the 16 keV line at  $\phi \sim 0.9-1.1$  may be in the anti-pencil beam. It is important to note that a part of the pencil-like beam (marked in ‘B’) produces a narrow anti-pencil beam, while the rest part acts as a hollow pencil-like beam (marked in ‘A’). Right: detailed structure of the accretion column. Two line-formation regions are shown in this figure. The line-formation region of the 12 keV line has a height of  $\sim 1$  km above the neutron star surface.